Front. Earth Sci. 2024, 18(4): 696−713
https://doi.org/10.1007/s11707-024-1111-4

RESEARCH ARTICLE

Gas charging and accumulation in deep coal measures of Daning-Jixian Block, Ordos Basin: insights from fluid inclusions and basin modeling

Zhanwei LI[1,2], Song LI (✉)[1,2], Dazhen TANG[1,2], Shuling TANG[1,2], Jiaosheng YANG[3], Wei HOU[4,5]

1 School of Energy Resources, China University of Geosciences (Beijing), Beijing 100083, China
2 Coal Reservoir Laboratory of National Engineering Research Center of CBM Development & Utilization, Beijing 100083, China
3 China Petroleum Exploration and Development Research Institute, Langfang 065007, China
4 National Engineering Research Center of China United Coalbed Methane Co. Ltd., Beijing 100095, China
5 PetroChina Coalbed Methane Company Limited, Beijing 100028, China

Abstract Unconventional natural gas in deep coal measures has become an exploration and research hotspot in recent years. The exploration breakthrough of deep coalbed methane and tight sandstone gas in Daning-Jixian Block in the eastern Ordos Basin has revealed huge resource potential and commercial prospects in the deep Upper Paleozoic Carboniferous-Permian coal measures. However, the ambiguity of gas accumulation in deep coal measures has restricted exploration and development. Based on a series of tests for fluid inclusions, including petrographic observation, Raman spectroscopy analysis, and microthermometry, combined with the burial-thermal evolution history recovered from basin modeling, this study aims to clarify the timing of gas accumulation in deep coal measures. The results show four types of secondary fluid inclusions in the deep coal measure sandstone layers of Daning-Jixian Block, including CH_4-rich inclusions, C_{2+} hydrocarbons-bearing inclusions, CO_2-bearing inclusions, and aqueous inclusions. The main formation stage of fluid inclusions corresponded to the mesodiagenesis stage of the deep coal measure sandstone, and the coeval assemblages of fluid inclusions vary due to the recording of gas charging in different maturity stages of coal measure source rocks. This study suggests that tight sandstone gas accumulation in deep coal measures was a continuous charging process with one period-multiple episodes in Daning-Jixian Block, and occurred mainly during the Early Cretaceous (137−127 Ma BP). The results of this study contribute to further understanding of gas accumulation mechanisms in deep coal measures.

Received August 10, 2023; accepted December 10, 2023

E-mail: lisong@cugb.edu.cn

Keywords gas accumulation, deep coal measures, fluid inclusions, basin modeling, Daning-Jixian Block

1 Introduction

With the increase of energy demand and exploitation, over-utilization and consumption of shallow high-quality oil and gas reserves, coal measure gas (CMS) with huge resource potential in deep coal measure strata, including coalbed methane (CBM), shale gas (SG), tight sandstone gas (TSG), etc., has attracted increasing attention (Bustin and Bustin, 2016; Qin, 2018; Ouyang et al., 2018; Zou et al., 2019; Shen et al., 2021; Tang et al., 2022). There is a significant amount of deep CMS resources in China, of which the CBM resources buried at 1000−2000 m account for 62.81% of the total 30.5 × 10^{12} m^3 of CBM resources buried above 2000 m (Zhang et al., 2018; Tao et al., 2019), and the resources of TSG and SG in deep coal measures are at least 1.5 times of CBM resources, which is a realistic choice for increasing gas reserves and production as well as ensuring energy-supply (Qin et al., 2022). Multi-stage and multi-cycle coal-mudstone-sandstone interbed sediments of the Carboniferous-Permian (C-P) coal measures in the eastern margin of Ordos Basin are favorable for the extensive development of CMS, thus becoming one of the hot areas for exploration and development in recent years (Zhao et al., 2014; Tang et al., 2018; Kuang et al., 2020; Zhang et al., 2021; He et al., 2022).

As one of the key CBM development blocks with abundant resources in the eastern margin of Ordos Basin, Daning-Jixian Block has achieved large-scale exploration and development of CBM with burial depth above 1500 m

with over 20 years evaluation (Li et al., 2018a; Zhang et al., 2022a) and several years production of TSG in the C-P coal measures with burial depth below 1500 m (Guo et al., 2018). Simultaneous studies on SG were carried out as well (Zeng et al., 2022; Zhang et al., 2022b). During the progressive exploration and development after the breakthrough of TSG exploration, several completed wells revealed multilayer gas-bearing tight sandstones in the C-P coal measures achieved commercial gas flow, with the maximum daily single-well gas production reaching 2×10^4 m^3 after fracturing (Li et al., 2018b), which demonstrated the great commercial prospects of the Upper Paleozoic tight sandstones. In recent years, a series of trial production tests of deep CBM with burial depth below 2000 m have been conducted in the deep joint exploration and development area of the block based on a number of old TSG wells, achieving a maximum daily gas production exceeding 2×10^4 m^3 from vertical wells and exceeding 10×10^4 m^3 from horizontal wells after fracturing, and proved the first 100×10^9 m^3 class deep CBM field with cumulative proved geological reserves of 112.1×10^9 m^3 in China (Yan et al., 2021; Xu et al., 2022). However, the overall exploration and understanding of deep CMS in Daning-Jixian Block are still premature, and the gas charging time and accumulation period in deep coal measures are not clear, which further limits exploration and development.

Fluid inclusions (FIs) are independent closed systems formed by capturing the original sedimentary and diagenetic fluids during the growth of mineral crystals and sealing them in diagenetic authigenic mineral cavities or diagenetic healing fractures (McLimans,1987; Goldstein, 2001; Munz, 2001). They directly recorded the history of rock-forming and reservoir-forming fluids, and could be used as a reliable tool to study the period and process of hydrocarbon accumulation in hydrocarbon-bearing basins (Pedersen and Christensen, 2007; Volk and George, 2019). In addition, Laser Raman micro-spectroscopy (LRM) has been widely used for the qualitative and semiquantitative analysis of the composition of individual FIs, especially gaseous hydrocarbon-containing inclusions (Burke, 2001; Frezzotti et al., 2012). Thus, it has been well accepted to determine the hydrocarbon charging time and accumulation period according to the homogenization temperature characteristics of aqueous inclusions associated with hydrocarbon inclusions in combination with the regional burial history and thermal history based on the types and assemblage characteristics of FIs (Xu et al., 2011; Fall et al., 2012; Bourdet et al., 2019; Shu et al., 2019; Cao et al., 2022).

In this study, the characteristics and types of FIs from different Upper Paleozoic sandstone layers in Daning-Jixian Block were defined based on detailed observation and analysis of the petrographic characteristics of FIs and component analysis of individual FIs by LRM. Analysis was further carried out for microthermometry of FIs and the burial-thermal evolution history of one typical well reconstructed through basin modeling to clarify the charging time and accumulation period of TSG in deep coal measures in the study area.

2 Geological setting

The Ordos Basin is a multi-rotation superimposed basin in western north China, and it can be divided into six primary tectonic units (Fig. 1(a)), including the Yimeng Uplift, Western Margin Thrust Belt, Tianhuan Depression, Yishaan Slope, Jinxi Flexural Fold Belt, and Weibei Uplift (Shen et al., 2021). The Daning-Jixian Block is located in the southern part of the eastern margin of Ordos Basin, with a total area of 5648 km^2, with the Huang He (Yellow R.) flows through the block from north to south along its western side. The block straddles the Yishaan Slope and Jinxi Flexural Fold Belt, showing the structural pattern of "one uplift, one depression and two slopes" (Zhang et al., 2022a), with the eastern slope belt (Mingzhu slope belt), Puxian depression belt, Taoyuan anticline belt, and Western gentle slope belt (Daning slope belt) successively distributed from the east to west (Fig. 1(b)). The localized north-eastern-orienting associated faults are widely developed between the Puxian depression belt and Taoyuan anticline belt, which increase the complexity of the local tectonic conditions (Li et al., 2019a). The joint exploration and development area of deep CBM and TSG is located in the Daning slope belt, characterized by a broad and gently west-dipping monocline, simple tectonics, undeveloped faults, and a stratigraphic dip angle of less than 2° (Yan et al., 2021).

The main strata revealed by field outcrops and drilling in Daning-Jixian Block are shown in Fig. 2, and the main coal-bearing strata are located in the Upper Carboniferous to Lower Permian Taiyuan Formation (C_2-P_1t) and Lower Permian Shanxi Formation (P_1s). Due to the long-term regional uplift, the thickness of sedimentary strata is relatively thin in Daning-Jixian Block, the average thickness of the C_2-P_1t and P_1s is about 80 m and 120 m, respectively.

During the Late Carboniferous to Middle Permian, the sedimentary environment of Daning-Jixian Block changed from marine-continental transitional facies to continental facies, forming the offshore-type C-P coal measures (Lu et al., 2012; Shao et al., 2018, 2020), where CBM, TSG, and SG are developed in multiple layers (Li et al., 2019b; Kuang et al., 2020; Yan et al., 2021). The widely distributed, thick coal seams and organic-rich mudstone/shale of the C-P coal measures are important hydrocarbon source rocks for deep CMS in the block (Zeng et al., 2022). The total thickness of the C-P coal seams ranges from 6.8 m to 22.8 m, of which No. 8 coal

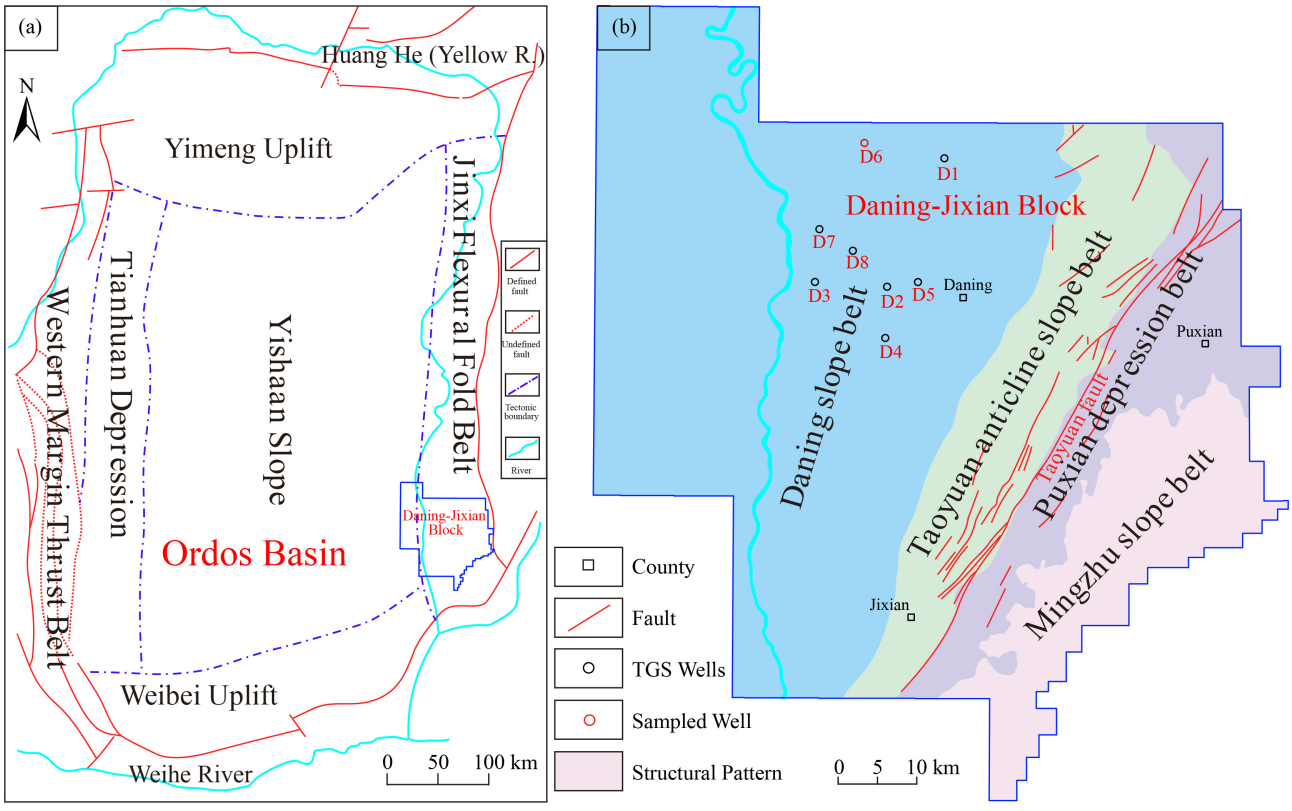

Fig. 1 Location and structural pattern of Daning-Jixian Block, south-eastern Ordos Basin. (a) Tectonic units of Ordos Basin and location of Daning-Jixian Block. (b) Structural pattern distribution map of Daning-Jixian Block (modified from Zhang et al., 2022b).

seam of the C_2-P_1t with a thickness of 2.4−12 m and No. 5 coal seam of the P_1s with a thickness of 1.5−12.3 m are the main coal seams as well as the targets for CBM exploration and development in Daning-Jixian Block (Yan et al., 2021). As the target layer of deep CBM, the main body of No. 8 coal seam has a burial depth of 2000−2520 m, with an average depth of 2130 m, while its thickness ranges from 5.2 m to 12.9 m, with an average of 7.8 m (Yan et al., 2021; Xu et al., 2022). The dominant tight sandstone reservoirs in the deep Upper Paleozoic in Daning-Jixian Block consist of the C_2-P_1t, Mbr (Member) 2 of the P_1s (P_1s_2), Mbr 1 of the P_1s (P_1s_1), and Mbr 8 of the Xiashihezi Formation (P_2h_8) sandstone layers from bottom to top (Fig. 2). These reservoirs are all dominated by ultra-low porosity with an average porosity lower than 7.0% and poor formation properties with average permeability in each layer ranging from 0.2 mD to 5.15 mD (Guo et al., 2018).

3 Sample preparation and methodology

3.1 Sample preparation

Well D6 was drilled through the Upper Paleozoic strata and completed in the Middle Ordovician Majiagou Formation (O_2m) at a depth of 2300 m. It is a typical TSG exploration well located in the deep joint exploration area, north-west of Daning-Jixian Block to identify the development layers and gas-bearing properties of the Upper Paleozoic sandstone reservoirs and to get core samples for the gas-bearing layers. In this study, over ten borehole core samples were collected from Jinci sandstone of the C_2-P_1t, Beichagou sandstone of the P_1s_2, Tiemogou sandstone of the P_1s_1, and Luotuobozi sandstone of the P_2h_8, which are the main gas-bearing layers in the C-P coal measures of well D6. Doubly polished thin sections (~300 μm) were prepared from the six representative collected sandstone samples with burial depths ranging from 2011.7 m to 2210.9 m (Table 1), by cutting in a perpendicular direction to the bedding plane.

3.2 Methodology

3.2.1 FIs analysis

In this study, the measurement of FIs under optical microscope, LRM, and microthermometry were conducted in the State Key Laboratory of Ore Deposit Geochemistry, Institute of Geochemistry, Chinese Academy of Sciences. The analysis and operating procedure for petrographic microscopic observation and microthermometry are outlined by Goldstein and Reynolds (1994).

Petrographic microscopic observation The 18 doubly polished thin sections were systematically observed under the transmission light of a Leica DM2700P optical

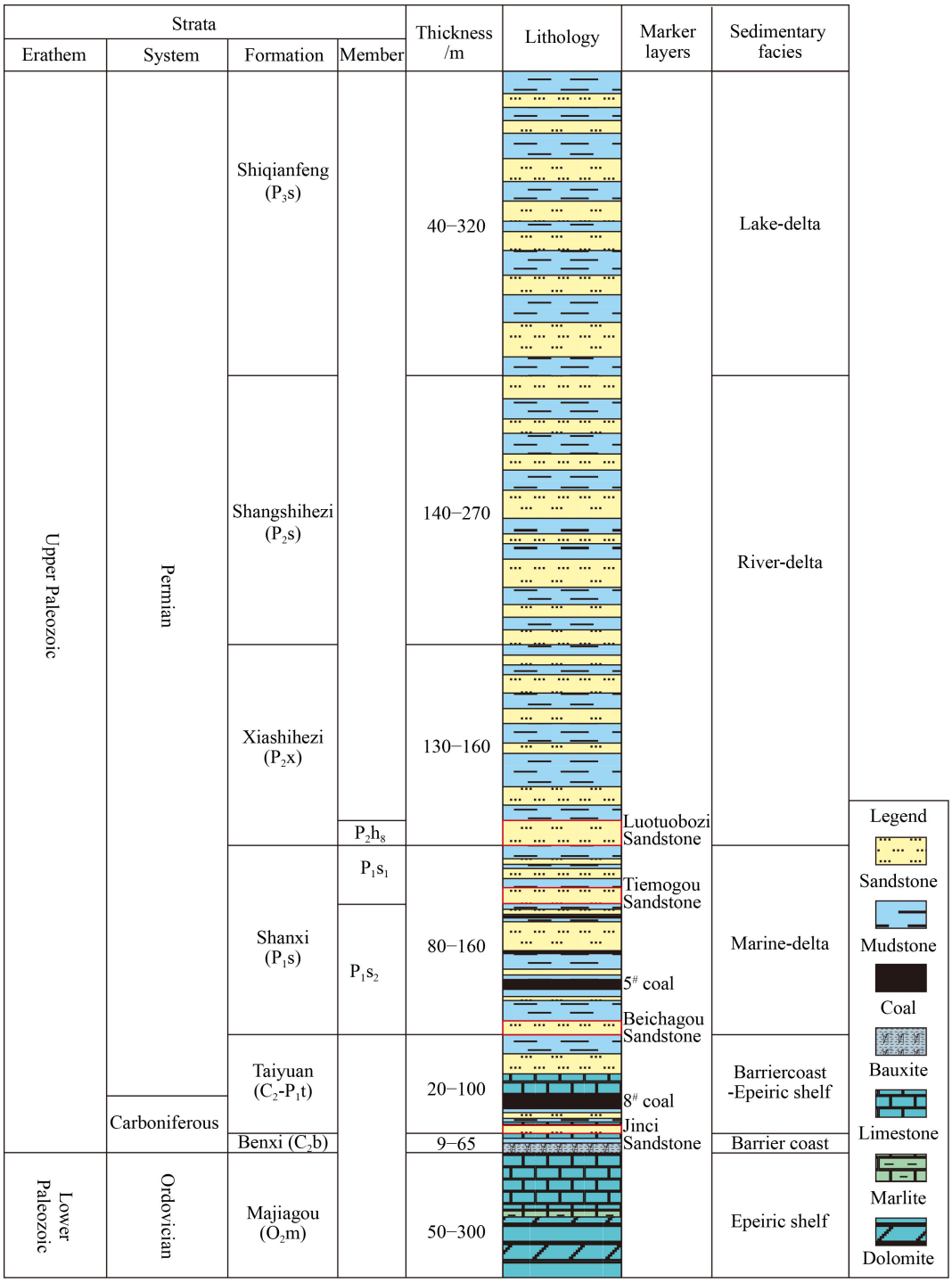

Fig. 2 Comprehensive stratigraphic column of the C-P coal measures in Daning-Jixian Block. Red boxes indicate selected sampling strata. Stratigraphic symbols refer to Zhao et al. (2014).

microscope to clarify the petrographic characteristics of the FIs, e.g., host mineral, occurrence, distribution, size, morphology, color, phase, and to select areas that contained more stable distribution, relatively regular morphology, and high abundance of inclusions.

Laser Raman micro-spectroscopy Raman micro-spectroscopy was performed on individual inclusions within the screened flake area with high-abundance using a LabRAM HR Evolution confocal laser Raman spectrometer (produced by HORIBA France SAS) to qualitatively identify the gaseous composition of FIs based on Raman spectrum characteristics and locate the effective mineral particles containing gaseous hydrocarbon inclusions and their coeval aqueous inclusions. The light source of the Raman spectrometer is a solid-state laser with a wavelength of 532 nm, power of 100 mW,

Table 1 Sample information of the Upper Paleozoic sandstones in Daning-Jixian Block.

Sample number	Depth/m	Formation	Lithology	Depositional environment
1	2011.7	P_2h_8	Grey fine-grained quartz sandstone	Delta-front underwater distributary channel
2	2072.8	P_1s_1	Gray fine-grained arkose sandstone	Delta-front underwater distributary channel
3	2076.5	P_1s_1	Gray fine-grained arkose sandstone	Delta-front underwater distributary channel
4	2140.8	P_1s_2	Grey fine-grained subarkose sandstone	Delta-front underwater distributary channel
5	2149.8	P_1s_2	Grey medium-grained subarkose sandstone	Delta-front underwater distributary channel
6	2210.9	C_2-P_1t	greyish white coarse-grained lithic quartz sandstone with gravels	Barrier bar

and linewidth of less than 1 nm. The output power of the laser beam on the sample surface is generally 25 mW, and the confocal effect can reach a spatial resolution of 1 μm. The spectrum was collected in the range of 100–4000 cm^{-1}, with an acquisition time of 10 s, and each spectrum was accumulated twice to improve the signal-to-noise ratio. The FIs with a size of 10–15 μm were screened, and the Raman spectrum was tested using a 600 grid/mm grating with a spatial resolution of 2 μm at laboratory temperature of 22°C and 65% humidity. To maintain the accuracy of the testing, the Raman spectrum was calibrated with a single crystal silicon standard sample before testing.

Microthermometry The homogenization temperature (T_h) and final ice melting temperature (T_m) of aqueous inclusions associated with hydrocarbon-bearing inclusions in the selected grains from thin sections were measured by using a calibrated Linkam THMSG600 heating-freezing stage (temperature range: −196°C to 600°C) in an environment maintained at 22°C with 60% humidity. The temperature control rate during T_h measurement was 1°C/min with a measurement precision of ± 0.2°C, while during T_m measurement, 0.1°C/min with a measurement precision of ± 0.1°C was applied. Recording T_h from low to high in microthermometric analysis to avoid overheating or stretching of FIs. To avoid the effect of later tectonic evolution on inclusions deformation, such as necking down, leakage, or stretching (Goldstein, 2001; Xu et al., 2016), 162 coeval aqueous inclusions, with small sizes (ranging from 4 μm× 3.1 μm to 32.7 μm× 5.1 μm, mostly concentrated under 15 μm× 10 μm) and low gas-liquid ratios (≤ 10%), were selected for microthermometry from thin sections of the Upper Paleozoic sandstone samples in Daning-Jixian Block.

3.2.2 Basin simulation analysis

One-dimensional (1-D) basin modeling was performed using PetroMod (version 2016) to reconstruct the burial-thermal history of well D6 in Daning-Jixian Block. Key input parameters are detailed in Table 2 as outlined by Yu et al. (2020). The model's geological time scales were derived from the chronostratigraphic framework of Ordos Basin combined with the stratigraphic chart of nearby regions (Yan et al., 2015; He et al., 2021), providing temporal constraints for depositional and erosional events. Data on geological stratification, lithologies, and present thicknesses were obtained from drilling and

Table 2 Key input parameters for 1-D basin modeling of well D6 in Daning-Jixian Block

Layer/Events	From/Ma	To/Ma	Base depth/m	Thickness/m	Erosion/m	Lithology
Q	2.58	0	60	60		Shale (sandy)
ER_4	125	2.58			1820	
ER_3	161	145			300	
ER_2	170	168			180	
ER_1	213	202			100	
T_3y	230	213	510	450		Sand & shale
T_2z	242	230	970	460		Sand & shale
T_1h	247	242	1104	134		Shale & sand
T_1l	251.9	247	1429	325		Shale & sand
P_3s	254	251	1678	249		Sand & shale
P_2x-P_2s	283	254	2051	373		Sand & shale
P_1s	295	283	2165	114		Coal & sand and shale
C_2-P_1t	307	295	2216	51		Coal & limestone &sand
C_2b	315	307	2257	41		Shale & limestone

logging activities. Notably, at least four erosion events occurred post the deposition of C-P coal measures, with the erosion thicknesses determined by referring to prior studies (Chen et al., 2006; Yu et al., 2017) and using mudstone acoustic travel time calculations (Yu et al., 2020).

The 1-D model's boundary conditions, including paleo-water depth (PWD), sediment-water interface temperature (SWIT), and heat flow (HF), are essential for basin modeling and must be determined in advance. PWD is primarily influenced by the paleo-sedimentary environment and can be estimated from the sedimentary sequence structure and sedimentary facies (Guo et al., 2022). SWIT was calculated using the global mean surface temperature model (Wygrala,1989) integrated within PetroMod software based on the location of the block (Eastern Asia, 36°N) and combined with PWD. HF in different geological periods were obtained from the results of previous studies in the literature (Wei et al., 2010; Yu et al., 2017; Ren et al., 2020).

In addition, the thermal history and organic matter maturity history of the C-P coal measures of well D6 were simulated by using the EASY%R_o model (Sweeney and Burnham, 1990). The 1-D model incorporated measured thermal metrics including vitrinite reflectance (R_o) of No. 8 coal seam, the T_h of FIs in the Upper Paleozoic sandstone samples, and the logging-derived temperature of well D6. During the modeling process, HF input values were continuously adjusted to obtain an optimal model with simulated values matching measured thermal metrics (Fig. 3). To estimate the peak palaeotemperature (T_{peak}) of the C-P coal measures in Daning-Jixian Block, a simple empirical correlation method (T_{peak} = [lnR_o + 1.68]/0.0124) proposed by Barker and Pawlewicz (1994) was used. Based on the measured R_o of No. 8 coal seam and the maximum T_h of aqueous inclusions associated with hydrocarbon-bearing inclusions in Jinci sandstone of the C_2-P_1t, it suggests that the maximum burial temperature of the C-P coal measure source rocks is not exceeding 230°C of well D6 in Daning-Jixian Block.

4 Results

4.1 Petrographic characteristics of fluid inclusions

Microscopic observations show a significant presence of FIs in the Upper Paleozoic sandstones in Daning-Jixian Block, with the host mineral generally dominated by quartz. The compaction was relatively strong in the Upper Paleozoic sandstones, and siliceous cementation was highly developed and quartz secondary enlargement can be easily observed (Figs. 4(a)–4(e)), some of the quartz grains even developed two-phase overgrowth rims (Figs. 4(c) and4(d)). These quartz clastic grains are typically encased by quartz overgrowths in various forms, such as semi-annular or annular shapes, and they generally exhibit uniform thickness. FIs are predominantly secondary in origin, as indicated by their presence in healed micro-fractures within quartz grains, quartz overgrowths, and micro-cracks cutting across quartz grains or their overgrowth rims (Fig. 4).

The distributions of FIs are diverse (Fig. 5), ranging from isolated, sporadic, and clustered distribution within quartz grains, to discontinuous bead and banded orientation arrangement along healed micro-fracture/crack, and ring ribbon patterns along quartz overgrowth rims. The

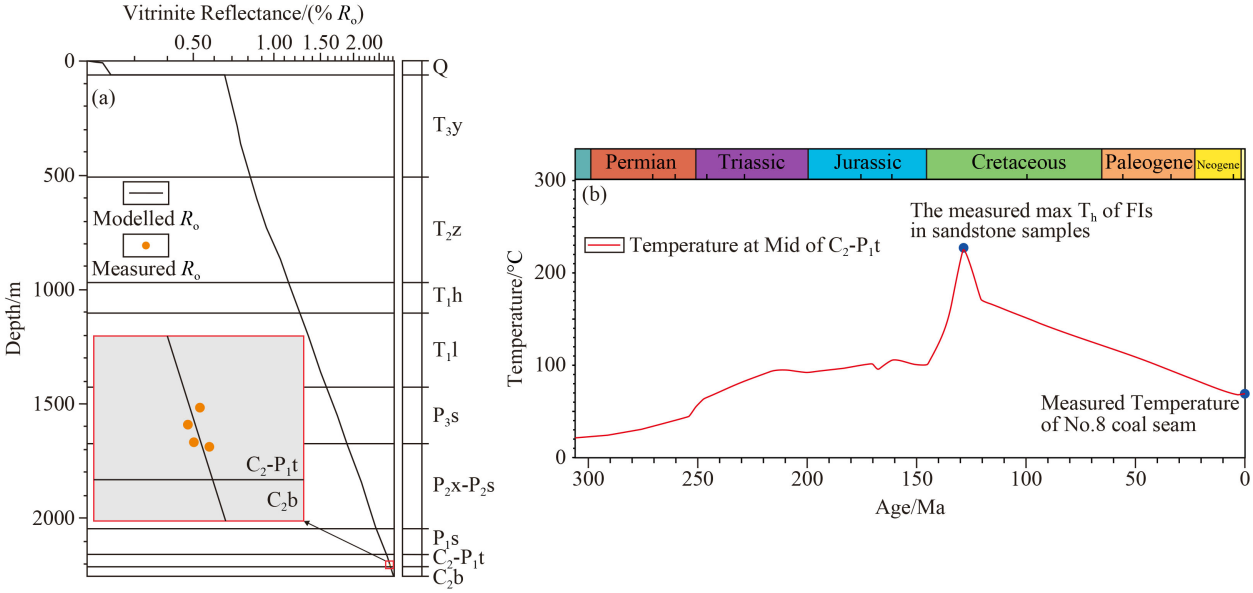

Fig. 3 Calibration on the thermal metrics in restoring the thermal evolution history of well D6. (a) The best fit between modeled R_o and measured R_o. (b) Variations of temperature versus time.

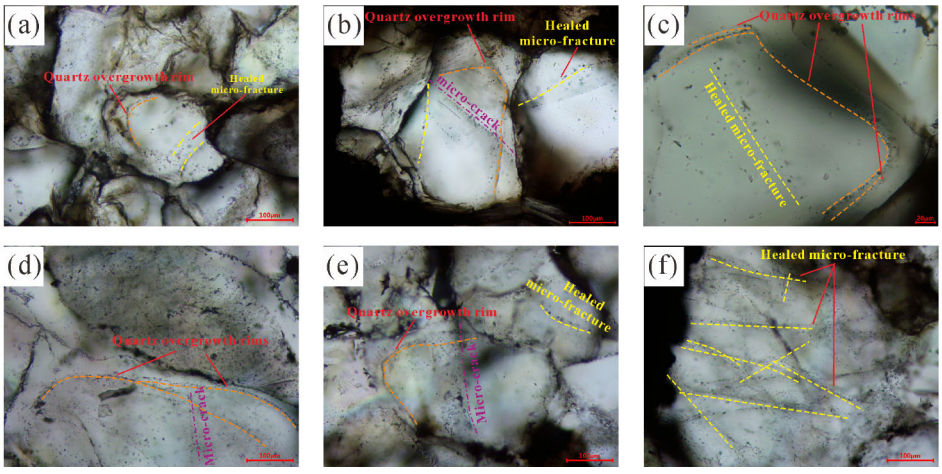

Fig. 4 Occurrence of FIs from different Upper Paleozoic sandstone layers in Daning-Jixian Block. (a) Healed micro-fracture and overgrowth rim of quartz, P_1s_1, 2072.8 m. (b) Healed micro-fracture, micro-crack cutting overgrowth rim of quartz grain, P_1s_1, 2076.5 m. (c) Two-phase quartz overgrowth rims, P_1s_2, 2140.8 m. (d) Two-phase quartz overgrowth rims, P_1s_2, 2149.8 m. (e) Healed micro-fracture, micro-crack cutting quartz grain and overgrowth rim, P_1s_2, 2149.8 m. (f) Reticulated healed micro-fracture within quartz grain, C_2-P_1t, 2210.9 m.

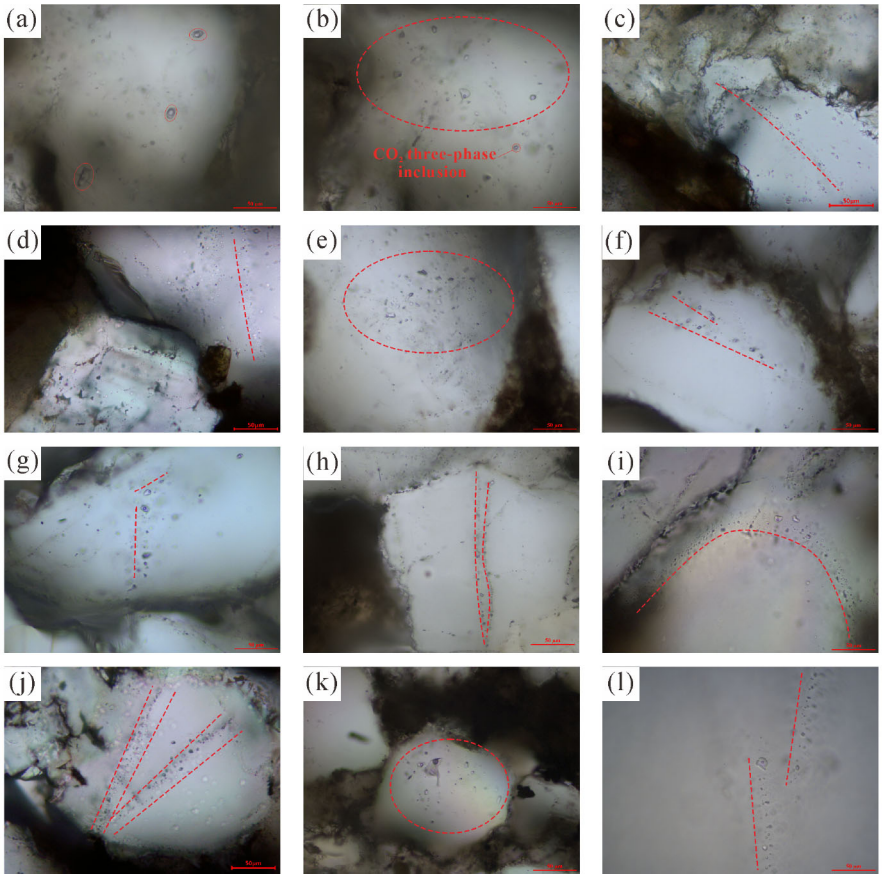

Fig. 5 Distributions of FIs from different Upper Paleozoic sandstone layers in Daning-Jixian Block. (a) Isolated distribution within quartz grain, P_2h_8, 2011.7 m. (b) Sporadic distribution within quartz grain, P_2h_8, 2011.7 m. (c) Discontinuous bead distribution crosses the quartz grain and overgrowths, P_1s_1, 2072.8 m. (d) Discontinuous bead distribution along healed micro-fracture within quartz grain, P_1s_1, 2072.8 m. (e) Clustered distribution within quartz grain, P_1s_1, 2076.5 m. (f) Discontinuous bead distribution along healed micro-fracture within quartz grain, P_1s_1, 2076.5 m. (g) Discontinuous bead distribution along healed micro-fracture within quartz grain, P_1s_2, 2140.8 m. (h) Discontinuous bead and nearly parallel distribution along healed micro-fracture within quartz grain, P_1s_2, 2140.8 m. (i) Ring ribbon distribution along quartz overgrowth rim, P_1s_2, 2149.8 m. (j) Banded distribution along healed micro-fractures within quartz grain, P_1s_2, 2149.8 m. (k) Clustered distribution within quartz grain, C_2-P_1t, 2210.9 m. (l) Discontinuous bead distribution along healed micro-fractures within quartz grain, C_2-P_1t, 2210.9 m.

shapes of these FIs are predominantly irregular, round, elliptical, spindle-like, or elongated, with sizes mostly between 6 and 12 μm, occasionally exceeding 30 μm. The size of individual inclusions varies significantly between and within sections.

At room temperature (22°C), the FIs exhibit diverse phase states and filling characteristics. These include vapor-liquid two-phase (vapor-rich or liquid-rich), pure vapor, and pure liquid phase inclusions, and occasionally three-phase inclusions. The most common are liquid-rich two-phase inclusions with small bubbles, typically having a gas-liquid ratio below 50%, and distinct gas-liquid boundaries. Under transmitted light, the bubble edges appear gray-black and thick, while the centers are translucent and shiny. The pure liquid-phase inclusions, generally smaller, appear lighter or colorless under transmitted light. Pure gas-phase inclusions are less frequent and less transparent, typically shiny in the center with gray-black peripheries, and sometimes entirely dark gray to gray-black. The vapor-rich two-phase inclusions, with larger bubbles and a gas-liquid ratio usually above 50%, are mostly shiny in the center with gray to dark gray edges under transmitted light. The three-phase inclusions, relatively large and light gray, appear as one bubble within another (Fig. 5(b)).

Generally, the petrographic characteristics of FIs in different Upper Paleozoic sandstone layers in Daning-Jixian Block show limited diversity. FIs can be generally categorized into two stages based on whether the secondary micro-crack containing inclusions cut through the quartz grains and its overgrowth. However, accurately categorizing the stages becomes challenging when multiple healed micro-fractures and micro-cracks are present.

4.2 Raman spectrum characteristics of fluid inclusions

The gaseous components of FIs were qualitatively identified according to the characteristic Raman spectrum (Xu et al., 2011; Frezzotti et al., 2012). High-intensity Raman characteristic peaks of quartz as the host mineral were visible in all measuring points. In addition, other typical Raman characteristic peaks were also detected for hydrocarbon gases including CH_4, C_{2+} hydrocarbons (referring to hydrocarbon gas with carbon atom number $\geqslant 2$, such as C_2H_6, C_3H_8), non-hydrocarbon gases (including CO_2, SO_2, N_2, CO) and liquid H_2O. All these indicate that the gaseous components in FIs of the Upper Paleozoic sandstones in Daning-Jixian Block are mainly CH_4 and C_{2+} hydrocarbons, followed by CO_2, and some even contain SO_2, N_2, and CO.

There are some variations in the gaseous components of FIs from different Upper Paleozoic sandstone layers in Daning-Jixian Block. For FIs in Jinci sandstone of the C_2-P_1t, along with the narrow and high-intensity characteristic peak of quartz, narrow and relatively low-intensity Raman characteristic peaks of CH_4 at 2913.1 cm^{-1} (Fig. 6(a)), CH_4 at 2917.1 cm^{-1} and SO_2 at 1159.7 cm^{-1} (Fig. 6(b)), and a gaseous mixture consisting of CH_4 at 2917.1 cm^{-1}, CO at 2133.4 cm^{-1}, SO_2 at 1158.5 cm^{-1} and N_2 at 2329.6 cm^{-1} can be observed (Fig. 6(c)), broad and variable intensity Raman peaks of H_2O were collected in all of them (Figs. 6(a)–6(c)). While for FIs in sandstones of the P_1s_2, single narrow and high intensity Raman characteristic peak of CH_4 occurred at 2911.4 cm^{-1} (Fig. 6(d)), the coexistence of relatively low intensity Fermi double peaks of CO_2 at 1281.0 cm^{-1} and 1385.5 cm^{-1} and lower intensity Raman characteristic peak of SO_2 at 1159.4cm^{-1} (Fig. 6(e)) or the hybrid gases of CH_4 at 2913.5 cm^{-1}, CO_2 at 1282.5 cm^{-1} and 1385.0 cm^{-1}, and SO_2 at 1156.5 cm^{-1} were detected (Fig. 6(f)). In sharp contrast to the P_1s_2, narrow and relatively very low intensity Raman characteristic peaks of C_2H_6 at 2950.7 cm^{-1}, CH_4 at 2917.6 cm^{-1}, and SO_2 at 1161.3 cm^{-1} were observed together in FIs in sandstones of the P_1s_1 (Fig. 6(g)), narrow and lower intensity peak of CH_4 at 2918.3 cm^{-1}, SO_2 at 1159.7 cm^{-1}, and wide stretching region of H_2O were also visible (Fig. 6(h)). As regards the FIs within sandstones of the P_2h_8, the results show that narrow and low intensity Raman characteristic peaks of CH_4 at 2917.1 cm^{-1}, relatively wide but lower intensity Raman characteristic peaks of C_{2+} hydrocarbons including C_2H_6 at 2964.2 cm^{-1} and other hydrocarbons at 1595.5 cm^{-1}, 1723.0 cm^{-1}, and 3072.2 cm^{-1}, respectively (Fig. 6(i)). Narrow and low intensity Raman characteristic peaks of C_{2+} hydrocarbons containing C_2H_6 at 2955.8 cm^{-1} and others at 1601.1 cm^{-1}, 1723.0 cm^{-1}, and 3075.0 cm^{-1}, respectively (Fig. 6(j)).

4.3 Microthermometry of fluid inclusions

The T_h of coeval aqueous inclusions is often regarded as indicative of the trapping temperature (Munz et al., 2004; Xu et al., 2011; Guo et al., 2022). Because aqueous inclusions coexisting with hydrocarbon-bearing inclusions in hydrocarbon basins have relatively low formation temperatures and stable components. Consequently, the T_h values of coeval aqueous inclusions do not significantly deviate from the trapping temperatures of FIs. The initial melting temperature values of these coeval aqueous inclusions measured were higher than −20.8°C, indicating that the saline solution in aqueous inclusions of the Upper Paleozoic sandstones in this block belongs to NaCl-H_2O system (Cao et al., 2022). Therefore, after removing a small portion of data with T_m exceeding 0°C due to the dissolution of light hydrocarbons and CO_2 (Chen et al.,2003), microthermometric data of the coeval aqueous inclusions (T_m between −21.2°C to 0°C) were interpreted using HokieFlincs_H_2O-NaCl Excel sheet (Steele-MacInnis et al., 2012) to obtain the salinity values of saline solution, which was estimated as wt.% NaCl equivalent (wt.% NaCl eq) (Bodnar, 1993).

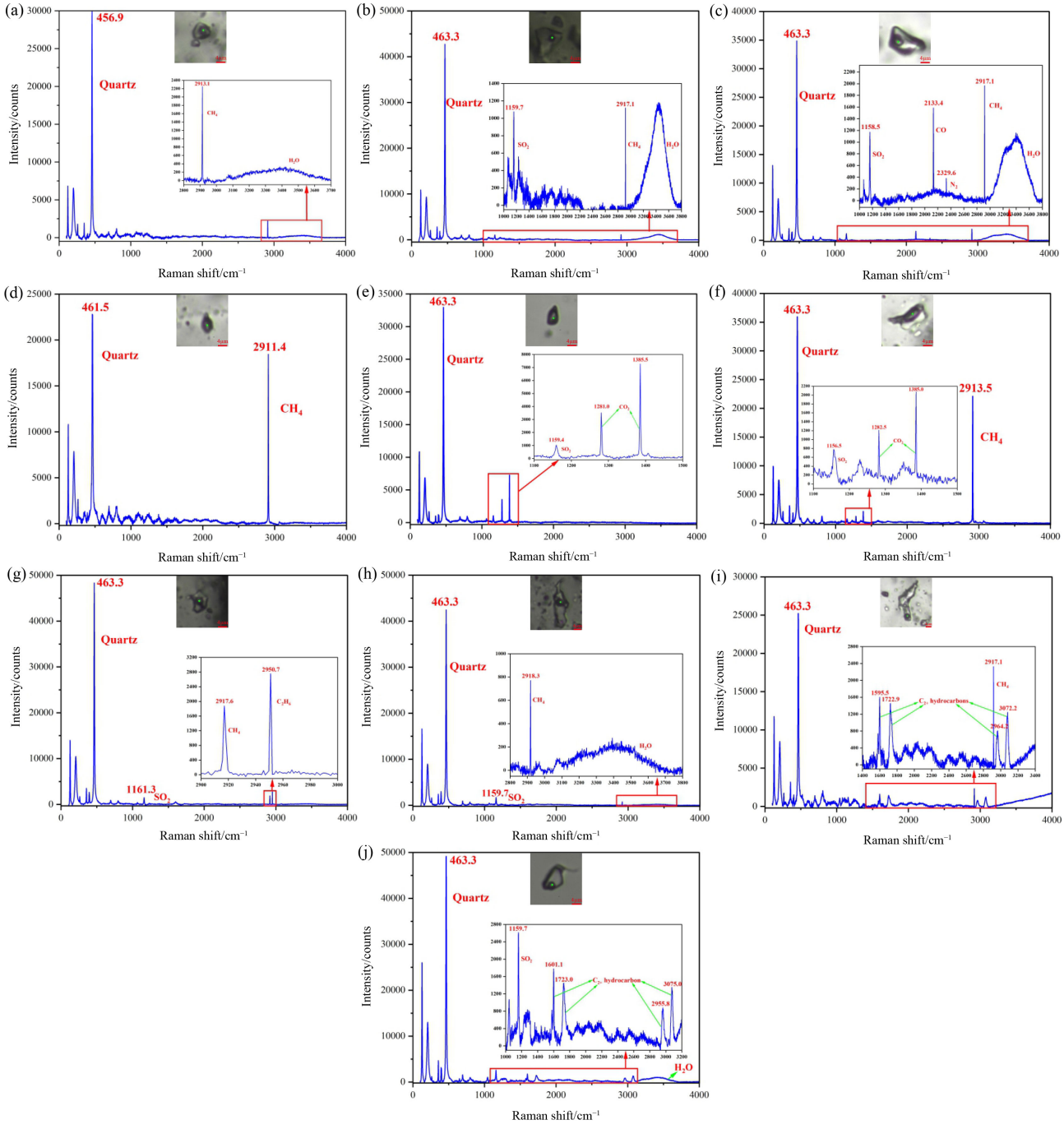

Fig. 6 Typical Raman spectrum of vapor bubbles in FIs from different Upper Paleozoic sandstone layers in Daning-Jixian Block. (a) Spectrum of CH_4 and H_2O collected in quartz, C_2-P_1t, 2210.9 m. (b) Spectrum of CH_4, SO_2 and H_2O collected in quartz, C_2-P_1t, 2210.9 m. (c) Spectrum of CH_4, CO, SO_2, N_2 and H_2O collected in quartz, C_2-P_1t, 2210.9 m. (d) Spectrum of CH_4 collected in quartz, P_1s_2, 2140.8 m. (e) Spectrum of CO_2 and SO_2 collected in quartz, P_1s_2, 2140.8 m. (f) Spectrum of CH_4, CO_2 and SO_2 collected in quartz, P_1s_2, 2149.8 m. (g) Spectrum of CH_4, C_2H_6 collected in quartz, P_1s_1, 2076.5 m. (h) Spectrum of CH_4, SO_2 and H_2O collected in quartz, P_1s_1, 2076.5 m. (i) Spectrum of CH_4, C_{2+} hydrocarbons collected in quartz, P_2h_8, 2011.7 m. (j) Spectrum of CH_4, C_{2+} hydrocarbons and H_2O collected in quartz, P_2h_8, 2011.7 m. The solid green points represent measurement points of LRM.

Overall, the coeval aqueous inclusions of the Upper Paleozoic sandstones in Daning-Jixian Block exhibit a broad range of T_h distribution, ranging from 110°C to 280°C, with three approximate peak temperature intervals of 130°C–160°C, 170°C–190°C, and 200°C–230°C, and mainly concentrated between 130°C and 160°C (Fig. 7(a)). T_h of a small number of aqueous inclusions exceeds the T_{peak} (~ 230°C), which could be explained as follows: (i) belong to primary inclusions, reflecting the temperature when the parent rock minerals were formed in the

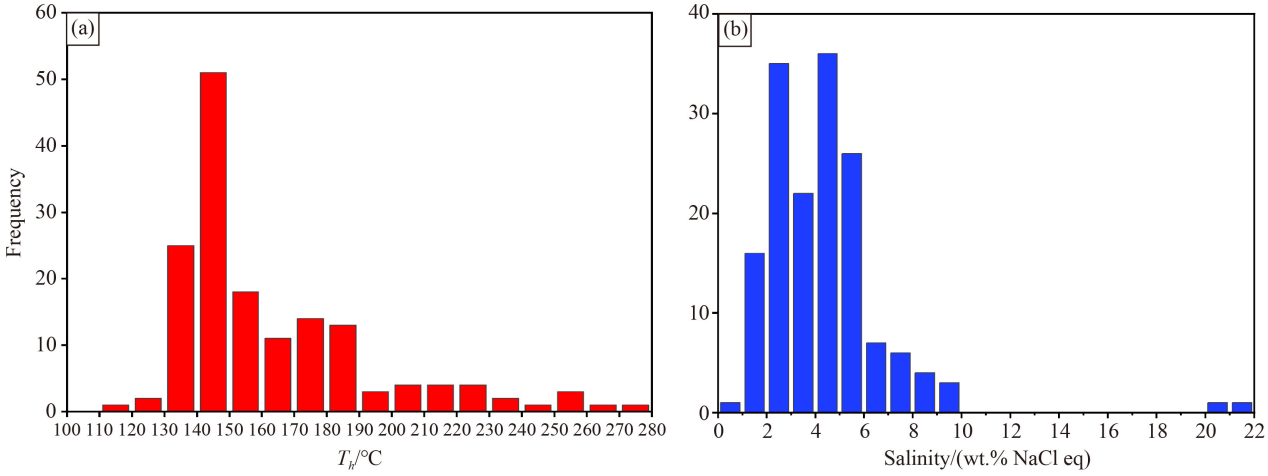

Fig. 7 Histogram of T_h and salinity of coeval aqueous inclusions of the Upper Paleozoic sandstones in Daning-Jixian Block. (a) T_h; (b) Salinity.

provenance area; (ii) affected by the mixing of deep hydrothermal fluid; and (iii) re-equilibration had occurred after the inclusions formed resulting in an increase in volume and T_h (Baron et al., 2008; Fall et al., 2012). Similarly, these aqueous inclusions also have a wide distribution of salinity between 0 and 22.0 wt.% NaCl eq. This salinity can be categorized into two peak intervals of 1.0−4.0 wt.% NaCl eq and 4.0−6.0 wt.% NaCl eq (Fig. 7(b)), respectively. Only two tested inclusions from the samples exhibited have salinity levels exceeding 20.0 wt.% NaCl eq, presumably due to the mixing of exotic high salinity fluids. Therefore, the data with T_h above 230°C or salinity over 20.0 wt.% NaCl eq (7 data, accounting for 4.3% of the total) were excluded during subsequent analysis.

The separate statistical analysis of T_h and salinity data of coeval aqueous inclusions from different Upper Paleozoic sandstone layers in the block are shown in Fig. 8. In the C_2-P_1t, T_h of coeval aqueous inclusions is continuously distributed between 142°C and 224°C with

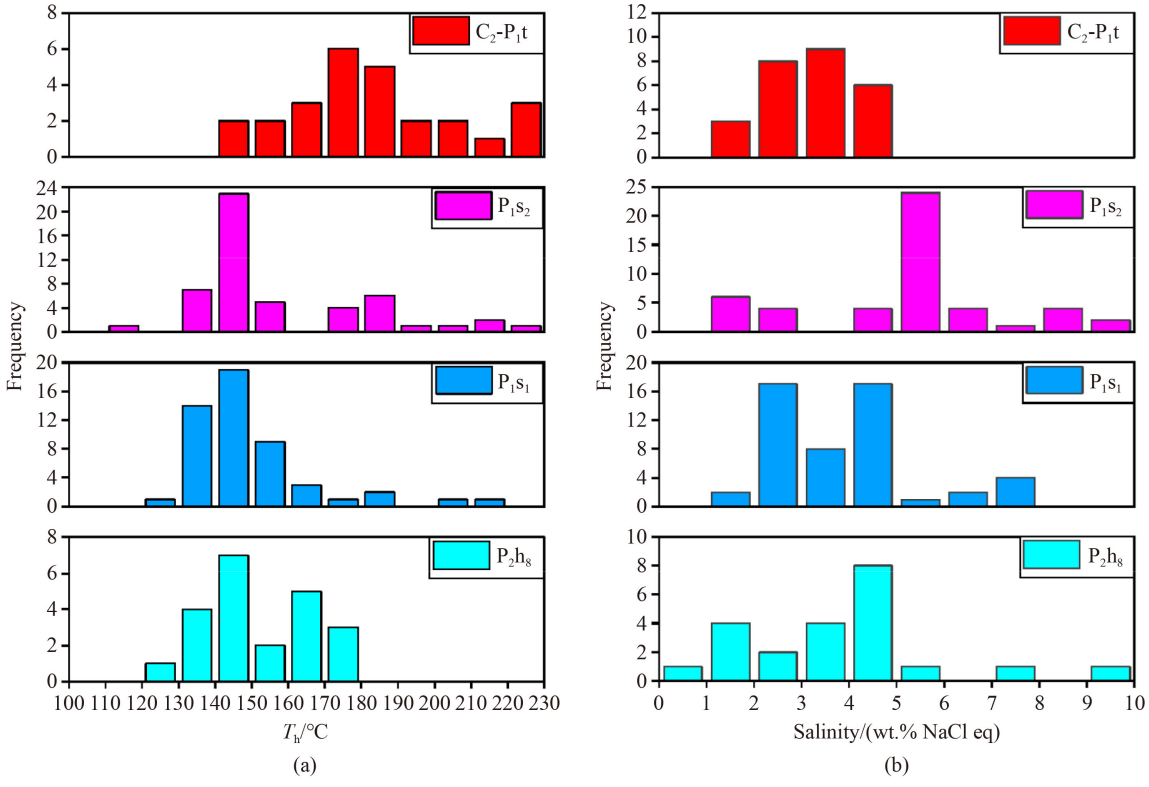

Fig. 8 Histogram of T_h and salinity of coeval aqueous inclusions in different Upper Paleozoic sandstone layers in Daning-Jixian Block.

the mean of 182°C and median of 181.5°C, which can be divided into two peak intervals of 170°C–180°C and 220°C–230°C, respectively, with the high-value interval is less pronounced. Its salinity is concentrated and continuously distributed between 1.6 and 4.3 wt.% NaCl eq with the mean of 3.1 wt.% NaCl eq and median of 3.1 wt.% NaCl eq, respectively. The approximate peak interval is 2.0–4.0 wt.% NaCl eq. In stark contrast, T_h of aqueous inclusions in the P_1s_2 is non-continuous distributed between 110°C and 223°C with a mean of 156°C and median of 147°C, as well as a well-defined peak interval between 140°C and 150°C. Similarly, its salinity is between 1.4 and 9.9 wt.% NaCl eq, with a mean of 5.2 wt.% NaCl eq and median of 5.4 wt.% NaCl eq, and a distinct single peak interval appears at 5.0–6.0 wt.% NaCl eq. For the P_1s_1, T_h of its aqueous inclusions is intermittently distributed in the range of 125°C–219°C, with a mean value of 149°C and median value of 143°C, identifying a definite peak interval of 140°C–150°C. While its salinity is continuously ranging between 1.6 wt.% NaCl eq and 7.6 wt.% NaCl eq with a mean of 3.9 wt.% NaCl eq and median of 3.7 wt.% NaCl eq, and two peak intervals in the ranges of 2.0–3.0 wt.% NaCl eq and 4.0–5.0 wt.% NaCl eq. Compared to the P_1s_1, the P_2h_8 has a continuous T_h distribution of aqueous inclusions ranging from 126°C to 175°C with a mean of 151.3°C and median of 148°C, respectively, along with two peak intervals 140°C–150°C and 160°C–170°C. However, its salinity is intermittently spread in the range of 0.7–9.2 wt.% NaCl eq with a mean value of 3.8 wt.% NaCl eq and median value of 3.95 wt.% NaCl eq, presenting two peak intervals of 1.0–2.0 wt.% NaCl eq and 4.0–5.0 wt.% NaCl eq, of which the former is not significant.

Regarding the correlation between T_h and salinity of coeval aqueous inclusions from different Upper Paleozoic sandstone layers in Daning-Jixian Block, the data exhibit a dispersed and irregular distribution (Fig. 9). Taking T_h of 150°C and salinity of 5.0 wt.% NaCl eq as the boundary, the coeval aqueous inclusions were grouped. They were called into one group characterized by high-temperature and low-salinity (zone IV) in the C_2-P_1t, and two combined groups for the other three layers. For the P_1s_2, they belong to mid-high-temperature and high-salinity (zone I) and high-temperature and composite-salinity (zone II and IV), and that of the P_1s_1 pertain to medium-high temperature and low-salinity (zone III) and high-temperature and composite-salinity (zone II and IV). Regarding the P_2h_8, they fall into medium-high temperature and low-salinity (zone III) and high-temperature and low-salinity (zone IV) .

4.4 Burial-thermal evolution history

Utilizing geological parameters such as drilling lithologies and erosion thickness, the burial-thermal evolution history of the C-P coal measures of well D6 in Daning-Jixian Block has been reconstructed (Fig. 10). According to the simulated burial evolution history of well D6, the burial evolution of the C-P coal measures can be divided into five distinct stages, including coal measures deposition, rapid subsidence, fluctuating uplift, secondary rapid subsidence, and continuous uplift, with the overall burial history curve that approximates an irregular “W” shape. The organic matter maturity within the C-P coal measures varied with their burial-thermal evolution history evolution.

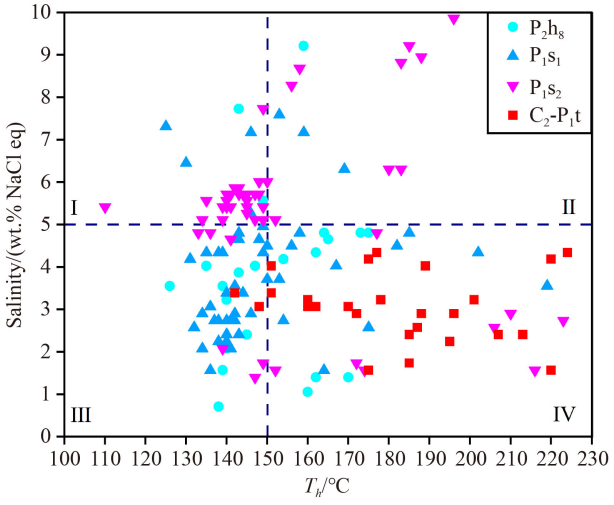

Fig. 9 Correlation relationship between T_h and salinity of coeval aqueous inclusions from different Upper Paleozoic sandstone layers in Daning-Jixian Block. I: Mid-high-temperature and high-salinity zone; II: High-temperature and high-salinity zone; III: Mid-high-temperature and low-salinity zone; IV: High-temperature and low-salinity zone.

I) Coal measures deposition stage

The Hercynian orogeny in the Late Carboniferous period turned the eastern Ordos Basin into a subsidence state and sedimentation began (Yan et al., 2015). Until the Early Permian, continuous sedimentation formed the C-P coal measures and the buried depth slowly increased. At this time, the shallow coal measures buried with temperature below 50°C, thus organic matter in the coal measures was immature.

II) Rapid subsidence stage

From the end of the Permian to the middle Late Triassic, rapid subsidence led to the deposition of continuous sedimentary strata of about 1800 m, and the burial depth of the C-P coal measures significantly increased, reaching a maximum depth of about 2500 m at the middle of the Late Triassic. Due to the long-term continuous burial, the temperature of the coal measures gradually increased and experienced long-term normal burial metamorphism. When the maximum burial depth at the middle Late Triassic is reached, the temperature of the coal measures was 90°C－96°C, R_o reached 0.5%–0.6%, and the coal measures entered the hydrocarbon generation threshold and began to generate hydrocarbons.

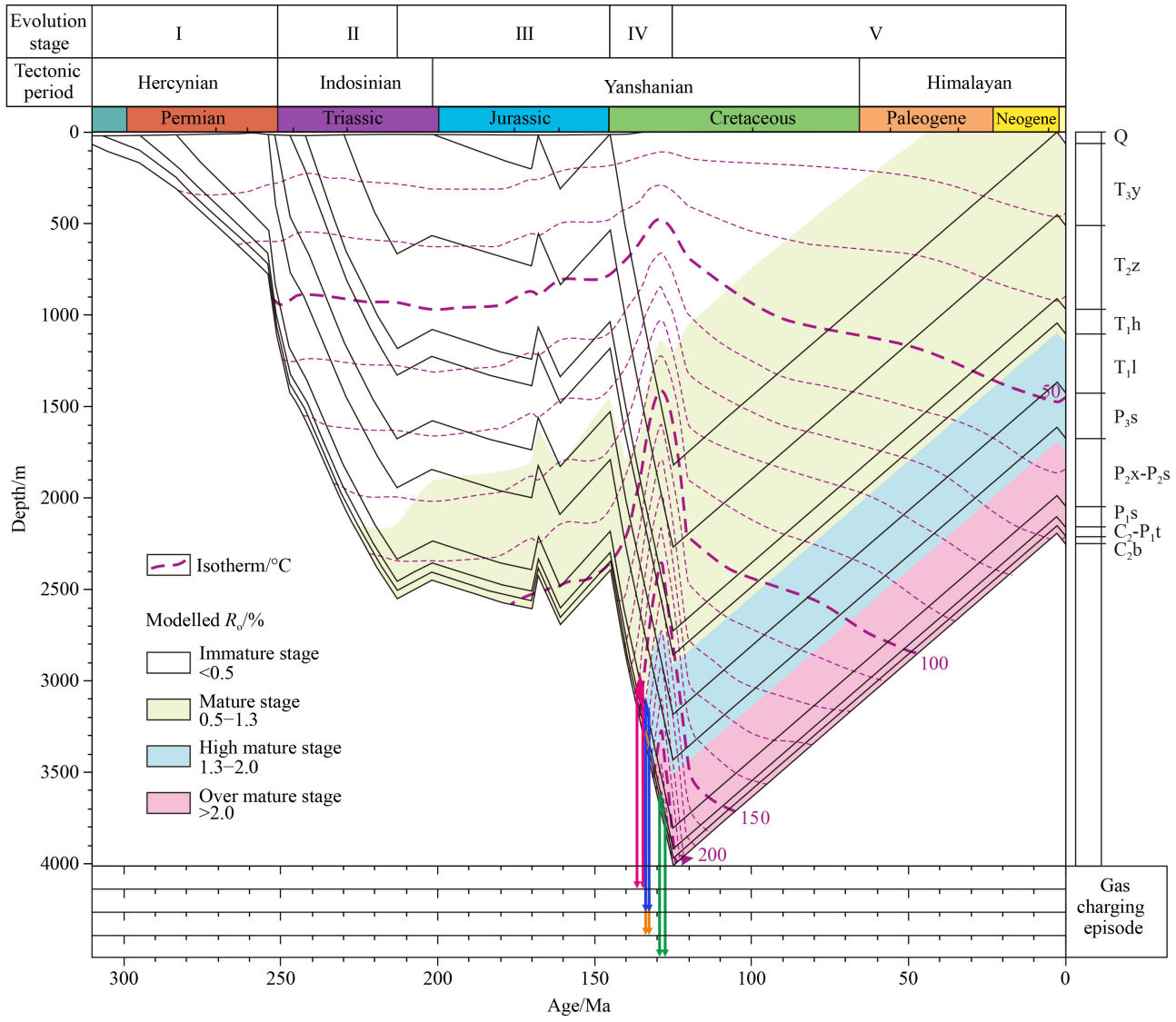

Fig. 10 The burial-thermal evolution history and gas charging episodes in deep coal measure sandstone layers of well D6 in Daning-Jixian Block. Stratigraphic notation: C_2b = Late Carboniferous Benxi Formation; C_2-P_1t = Late Carboniferous to Early Permian Taiyuan Formation; P_1s = Early Permian Shanxi Formation; P_2x-P_2s = Middle Permian Xiashihezi Formation to Shangshihezi Formation; P_3s = Middle Permian Shiqianfeng Formation; T_1l = Early Triassic Liujiagou Formation; T_1h = Early Triassic Heshanggou Formation; T_2z = Middle Triassic Zhifang Formation; T_3y = Late Triassic Yanchang Formation; Q = Quaternary.

III) Fluctuating uplift stage

During this stage, influenced by the Indosinian orogeny and the Early Yanshanian orogeny, the C-P coal measures presented an uplifting trend, and the maximum burial depth reaching to about 2350 m, although it experienced two deposition and three erosion events during the period. The temperature of the coal measures varied with the burial depth during this stage, and the thermal evolution of organic matter was comparatively slow. By the end of this stage, in the Early Cretaceous, the temperature of the coal measures was between 93°C to 100°C, and R_o reached 0.6%−0.7%.

IV) Secondary rapid subsidence stage

During the Early Cretaceous period, the study area was deposited rapidly again due to the impact of the Middle Yanshanian orogeny, which led to the significant increasing of buried depth of the C-P coal measures to the maximum burial depth of approximately 4000 m. Superimposed on the influence of an anomalous high-temperature field caused by a regional tectonic thermal event (Yu et al., 2017), the temperature of the coal measures increased significantly. Meanwhile, the thermal evolution of organic matter in the coal measures accelerated rapidly and entered the secondary hydrocarbon generation stage (Wei et al., 2010). When the maximum burial depth was reached, the temperature of the coal measures reached approximately 210°C−230°C, while R_o reached 2.6%−2.8%.

V) Continuous uplift stage

Following the Early Cretaceous, the study area experienced strong uplift and erosion events due to effects of the Late Yanshanian and Himalayan orogenies. This geological activity prompted the continuous uplift of the C-P coal measures. Despite some short-term depositional episodes since the Quaternary, their impact on the burial depth of the coal measures was minimal. Currently, the maximum burial depth has stabilized at approximately 2100–2215 m. The extensive uplift of the coal measures, coupled with the massive erosion of the overlying strata, resulted in a significant decrease in formation temperature, and the termination of organic matter maturation in the coal measures resulted in no obvious change in R_o.

5 Discussion

5.1 Types of fluid inclusions

Based on a comprehensive analysis of the petrographic characteristics and Raman spectrum characteristics, the secondary FIs in the Upper Paleozoic sandstones in Daning-Jixian Block can be subdivided into four distinct types. These include CH_4-rich inclusions, C_{2+} hydrocarbons-bearing inclusions, CO_2-bearing aqueous inclusions, and aqueous inclusions. However, the difference in the number of different types of FIs from the Upper Paleozoic sandstone layers may not be fully reflected, owing to the limitations in LRM measurements (Fig. 11).

CH_4-rich inclusions These inclusions predominantly contain CH_4, with minimal or no presence of C_2H_6, CO_2, and SO_2 compared to the amount of CH_4. Both approximately pure gas phase and vapor-liquid two-phase are available, with two-phase predominating and individuals varying in size. The morphology of two-phase CH_4-rich inclusions is complex and dominated by irregular shape, with gas-liquid ratio between 10%–30%. Such inclusions are mainly developed along micro-crack cutting quartz grain and/or its overgrowth rim and distributed in discontinuous beads or belts (e.g., Figs. 5(c) and 5(j)). This type of inclusion is found in all the Upper Paleozoic sandstone layers, among which the C_2-P_1t and P_1s_2 are superior in number.

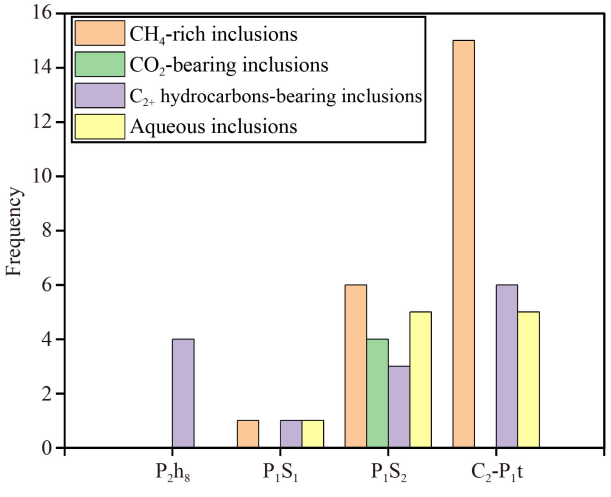

Fig. 11 Types of FIs from different Upper Paleozoic sandstone layers of Daning-Jixian Block.

C_{2+} hydrocarbons-bearing inclusions The gaseous components of these inclusions are mainly C_{2+} hydrocarbons, and some of them contain small amounts of CH_4 or SO_2. The majority are in a gas-liquid two-phase state, typically with the gas-liquid ratio of less than 10%, with gray to gray-black bubbles under translucent light (e.g., Figs. 5(e) and 5(k)). The morphology of individual inclusions is predominantly irregular, and their size varies considerably. These inclusions are discontinuous bead distribution in healed micro-fracture within quartz grains and ring ribbon distribution along the inner side of quartz overgrowth rims. They are variably developed across all Upper Paleozoic sandstone layers.

CO_2-bearing inclusions These inclusions are mainly in gas-liquid phase, with CO_2 as the dominant gas component. Some also contain a small amount of SO_2 or hydrocarbons. In general, the individuals are elliptical or circular in shape, larger in size with an average diameter of over 10 μm, and mostly are gray to gray-black under transmitted light. Some inclusions occurred as three-phase, consisting of gaseous CO_2, liquid CO_2 and saline solution, with relatively large individuals (e.g., Fig. 5(b)). The CO_2-bearing inclusions are mainly located in healed micro-fracture within quartz grains and early quartz overgrowths with low abundance in all the Upper Paleozoic sandstone layers.

Aqueous inclusions This type of inclusion has the highest abundance, mostly in the form of liquid-rich two-phase, diverse in shape, varying in size and are relatively small. These inclusions coexist with hydrocarbon-bearing inclusions, which are colorless or light gray under transmitted light. Such inclusions are distributed in quartz overgrowths and healed micro-fracture within quartz grains as discontinuous beads or clusters (e.g., Figs. 5(d), 5(i), and 5(l)). This type of inclusion is well developed in all the Upper Paleozoic sandstone layers in the block.

5.2 Fluid evolution of fluid inclusions

Consistent with trends observed in the eastern Ordos Basin (Su et al., 2021; Zhang et al., 2022c), the Upper Paleozoic sandstones have undergone various diagenetic processes. These processes include compaction and compression, dissolution of unstable components, and cementation of carbonate, siliceous, and clay minerals in Daning-Jixian Block. Therefore, the sandstone layers of the P_2h_8 to the C_2-P_1t had successively experienced multiple diagenetic stages, including eodiagenesis stage,

mesodiagenesis stage A, mesodiagenesis stage B, and now generally evolved into the late diagenesis stage in accordance with the China petroleum and natural gas sector standard of "The Division of Diagenetic Stages in Clastic Rocks" (SY/T 5477-2003).

During the eodiagenesis stage (R_o < 0.5%, paleotemperature < 85°C), compaction was the predominant process in the target stratum of the block, with some development of siliceous cementation. However, overall cementation remained weak, which was not conducive to the formation of FIs. From the Middle Triassic to the Early Cretaceous, with the fluctuating increase in burial depth, the target strata evolved into the mesodiagenesis stage A (0.5% < R_o < 1.3%, 85°C < paleotemperature < 140°C). During this period, the dissolution of unstable minerals such as feldspar and rock debris in the acidic fluid environment formed by the dissolution of organic acids (carboxylic acid) and CO_2 generated during hydrocarbon generation of the C-P coal measure source rocks, provided large amounts of Si^{4+} for the formation of quartz secondary enlargement (Su et al., 2021). Meanwhile, the organic matter in the coal measures evolved slowly into the mature stage, thus the FIs captured in healed micro-fractures and quartz overgrowths predominantly consisted of a paragenetic assemblage of CO_2-bearing inclusions, C_{2+} hydrocarbons-bearing inclusions, and aqueous inclusions. Subsequently, the target strata immediately progressed into the modiagenesis stage B (1.3% < R_o < 2.0%, 140°C < paleotemperature < 175°C) during the Early Cretaceous. During this period, the acidity of the fluid environment in the coal measures became weaker and converted to medium and alkaline, with diagenesis mainly manifested by quartz secondary enlargement and microfracturing, so FIs formed in the process are primarily a combination of CH_4-rich inclusions and aqueous inclusions. Up to the late diagenesis stage (2.0% < R_o < 2.8%, 175°C < paleotemperature < 200°C), diagenesis was relatively weak (Li et al., 2020), and the thermal evolution of organic matter in coal measures entered the over mature stage. FIs captured at this period were predominantly CH_4-rich inclusions and aqueous inclusions, with significantly increased levels of CH_4 content, which were mainly distributed in micro-cracks.

In summary, the evolution of fluid components in FIs of the Upper Paleozoic sandstones proved that the formation stages of FIs in Daning-Jixian Block correspond to the hydrocarbon generation history of the Upper Paleozoic coal measure source rocks (Fig. 12), which is also consistent with previous findings in the Upper Paleozoic sandstones from other regions in the east margin of Ordos Basin (Xu et al., 2011; Shu et al., 2019; Cao et al., 2022).

5.3 Gas charging history

The T_h peak intervals were projected onto the burial-thermal evolution curve before the stratigraphic long-term uplift in the Early Cretaceous (~130−125 Ma BP) (Yan et al., 2015; Shu et al., 2019) for comparative analysis. The results show that gas accumulation in Daning-Jixian Block mainly occurred during the Early Cretaceous (Fig. 10). However, the timing of gas charging varied across different sandstone layers, influenced by their respective vertical distances from the coal measure source rocks (Fig. 13). The main T_h peak interval of the coeval aqueous inclusions in sandstone samples of the P_1s_2 to P_2h_8 are all 140°C−150°C, indicating that the gas charging time was approximately 137−135 Ma BP, corresponding to the early Early Cretaceous. Meanwhile R_o was in the range of 0.9%−1.1%, marking the large-scale charging of gaseous hydrocarbons generated from the early thermal degradation of organic matter from the Upper Paleozoic coal measure source rocks. In addition, for the other T_h peak interval of the P_2h_8 at 160°C−170°C, the gas charging probably occurred at 134−133 Ma BP, corresponding to the middle Early Cretaceous. At this time R_o was 1.4%−1.6%, which was in the high mature stage, marking the charging of gaseous hydrocarbon mixtures generated by thermal cracking of the coal measure source rocks. As for the C_2-P_1t, according to the T_h peak intervals of its coeval aqueous inclusions at 170°C−180°C and 220°C−230°C, it can be inferred that the gas charging time was approximately 134−133 Ma BP and 129−127 Ma BP, corresponding to the middle to late Early Cretaceous. In this process, R_o was 1.4%−1.6% of the high mature stage, marking the charging of gaseous hydrocarbon mixtures generated by thermal cracking of the coal measure source rocks. When R_o was 2.5%−2.7% of the over mature stage, marking the large-scale charging of CH_4-dominated gaseous hydrocarbons generated by thermal cracking of organic matter from the coal measure source rocks.

Furthermore, the salinity of the aqueous inclusions from the P_2h_8 to the P_1s_2 exhibits an increasing trend, while their T_h distribution remains relatively similar,

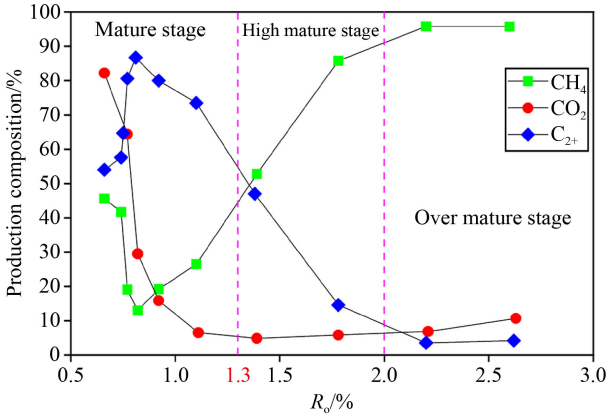

Fig. 12 Product composition of the Upper Paleozoic coal in different evolution stages of Ordos Basin (modified from Li et al., 2005).

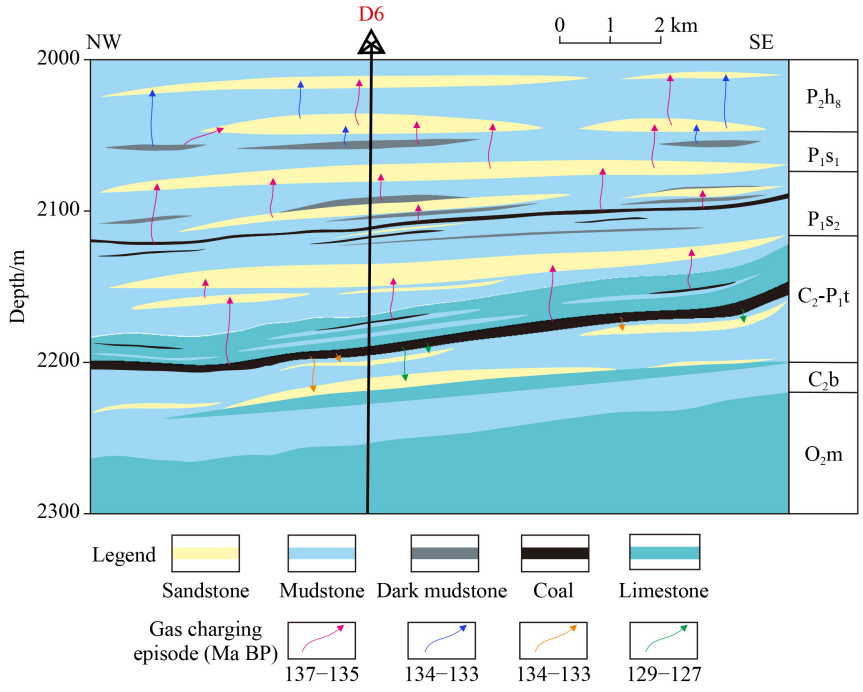

Fig. 13 Schematic diagram of gas charging in the deep coal measure sandstone of Daning-Jixian Block. "Gas charging episode" with the same color as in Fig. 10.

suggesting that the fluid properties within these layers are relatively homogeneous and well connected vertically, capturing FIs during the gas charging from bottom to up. Meanwhile, the lower layer captured the fluid with relatively high salinity as a result of increasing salt solubility in the formation water with temperature (Shu et al., 2019). The case of the C_2-P_1t indicates the initial formation water was a mixture of coastal saline water and terrestrial fresh water with relatively low salinity, and the injection of the compaction-released water of the coal measures also reduced its salinity. In addition, the Upper Paleozoic sandstone layers were compacted when the inclusion was captured, and a closed system was developed. The gas charging was achieved only when a large amount of hydrocarbon was generated in the high-over mature stages and accumulated near the coal measure source rocks, making the inclusions of the C_2-P_1t show low salinity and high T_h characteristics.

The T_h of FIs in the Upper Paleozoic sandstone layers in Daning-Jixian is continuously distributed without noticeable sparks (Fig. 7(a)), indicating that TGS charging in deep coal measures was a relatively continuous process without significant interruption. In view of the limited interval of charging time in different sandstone layers, it suggests that TSG accumulation in deep coal measures was a one period-multiple episodes process as the close source charging type (Li et al., 2021) in Daning-Jixian Block, and the main period of gas accumulation ranges from 137 Ma BP to 127 Ma BP, corresponding to the early to late Early Cretaceous.

6 Conclusions

Based on petrographic observations, Raman spectroscopy analysis, and microthermometry for FIs from different sandstone layers within the C-P coal measures (burial depth > 2000 m) in Daning-Jixian Block, and combined with the single well burial-thermal evolution history recovered from basin modeling, several key conclusions have been made.

1) The secondary FIs in the Upper Paleozoic sandstones of Daning-Jixian Block are abundantly distributed in the healed micro-fracture and overgrowths of quartz grains and micro-cracks. These inclusions have been classified into four types based on petrographic characteristics and Raman spectrum analysis: CH_4-rich inclusions, C_{2+} hydrocarbons-bearing inclusions, CO_2-bearing inclusions, and aqueous inclusions.

2) Currently, the Upper Paleozoic sandstones in Daning-Jixian Block have reached the late diagenesis stage. The formation of FIs predominantly corresponds to the mesodiagenesis stage A and B. The coeval assemblages of FIs differ across various periods, influenced by the varying maturity level of organic matter in the C-P coal measures.

3) The coeval aqueous inclusions of the Upper Paleozoic sandstones in Daning-Jixian Block present wide and smooth variations in T_h and salinity distribution. Distinct distributions of T_h and salinity are evident among different sandstone layers. The FIs of sandstone samples record the continuous gas charging process performed with one period-multiple episodes in different maturity

stages of coal measure source rocks. TGS accumulation in deep coal measures of Daning-Jixian Block mainly occurred in the Early Cretaceous (137−127 Ma BP).

Acknowledgment This study was supported by the National Natural Science Foundation of China (Grant Nos. 42130802 and 42072198), the Fundamental Research Funds for the Central Universities (No. 265QZ2021011), PetroChina Company Limited "14th Five Year Plan" Science and Technology Major Project (No. 2021DJ2301) and PetroChina Company Limited Science and Technology Project (No. 2023-KJ-18).

Competing interests The authors declare that they have no competing interests.

References

Barker C E, Pawlewicz M J (1994). Calculation of vitrinite reflectance from thermal histories and peak temperatures. In: Mukhopadhyay P K, Dow W G, eds. Vitrinite Reflectance as a Maturity Parameter: Applications and Limitations. American Chemical Society Symposium Series 570. Washington D C: American Chemical Society, 216–229

Baron M, Parnell J, Mark D, Carr A, Przyjalgowski M, Feely M (2008). Evolution of hydrocarbon migration style in a fractured reservoir deduced from fluid inclusion data, Clair Field, west of Shetland, UK. Mar Pet Geol, 25(2): 153–172

Bodnar R J (1993). Revised equation and table for determining the freezing point depression of H_2O-NaCl solutions. Geochim Cosmochim Acta, 57(3): 683–684

Bourdet J F R, Heath C H, Kempton R H (2019). Adaptation of fluid inclusion techniques for investigating gas charge—examples from the Caswell Sub-basin, Browse Basin, Australia. Special Publications, Vol 484, London: The Geological Society of London, 29–50

Burke E A J (2001). Raman microspectrometry of fluid inclusions. Lithos, 55(1−4): 139–158

Bustin A M M, Bustin R M (2016). Total gas-in-place, gas composition and reservoir properties of coal of the Mannville coal measures, Central Alberta. Int J Coal Geol, 153: 127–143

Cao Q, Wei X S, Chen Z X, Zhao J Z, Tang M J (2022). Hydrocarbon charge history of the Upper Paleozoic, Ordos Basin as revealed by fluid inclusions. Front Phys (Lausanne), 10: 836977

Chen H H, Wang J H, Xie Y H, Wang Z F (2003). Geothermometry and geobarometry of overpressured environments in Qiongdongnan Basin, South China Sea. Geofluids, 3(3): 177–187

Chen R Y, Luo X R, Chen Z K, Yu J, Yang Y (2006). Restoration of burial history of four periods in Ordos Basin. Acta Geol Sin, 27(2): 43–47 (in Chinese)

Fall A, Eichhubl P, Cumella S P, Bodnar R J, Laubach S E, Becker S P (2012). Testing the basin-centered gas accumulation model using fluid inclusion observations: southern Piceance Basin, Colorado. AAPG Bull, 96(12): 2297–2318

Frezzotti M L, Tecce F, Casagli A (2012). Raman spectroscopy for fluid inclusion analysis. J Geochem Explor, 112: 1–20

Goldstein R H (2001). Fluid inclusions in sedimentary and diagenetic systems. Lithos, 55(1−4): 159–193

Goldstein R H, Reynolds T J (1994). Systematics of Fluid Inclusions in Diagenetic Minerals. SEPM Short Course No. 31, Tulsa, Oklahoma, 199

Guo L L, Li Z B, Zhang W, Lin W J, Yang M M, Zhao Y (2018). Pore structure characteristics of tight sandstone in Daning-Jixian block, Ordos Basin. Nat Gas Ind, 38(S1): 18–23 (in Chinese)

Guo Y C, Cao J, Liu R Q, Wang H F, Zhang H Y (2022). Hydrocarbon accumulation and alteration of the Upper Carboniferous Keluke Formation in the eastern Qaidam Basin: insights from fluid inclusion and basin modeling. J Petrol Sci Eng, 211: 110116

He D F, Bao H P, Kai B Z, Wei L B, Xu Y H, Ma J H, Cheng X (2021). Critical tectonic modification periods and its geologic features of Ordos Basin and adjacent area. Acta Petrolei Sin, 42(10): 1255–1269

He Q B, Chen S J, Li S X, Guo B Z, Lu J G, Li Y, Li X G, Zhao L P, Ma Z W (2022). Organic geochemical characteristics and hydrocarbon generation mechanism of marine-continental transitional organic-rich shale: a case study from the Shanxi formation in the eastern margin of the Ordos Basin. J Petrol Sci Eng, 219: 111116

Kuang L C, Dong D Z, He W Y, Wen S M, Sun S S, Li S X, Qiu Z, Liao X W, Li Y, Wu J, Zhang L F, Shi Z S, Guo W, Zhang S R (2020). Geological characteristics and development potential of transitional shale gas in the east margin of the Ordos Basin, NW China. Pet Explor Dev, 47(3): 471–482

Li B J, Gao Y H, Zhou C F, Gu X J, Du C L, Gao L B (2018b). Integration technology of fracturing and gas test for tight sandstone gas reservoirs in Daning-Jixian block. Well Testing, 27(5): 56–60 (in Chinese)

Li C G, Jiang B, Ju W, Cheng G X, Song Y (2019a). Characteristics of tectonic deformation in the Daning-Jixian region, eastern Ordos Basin: implications for the exploration and development of coalbed methane. Energy Explor Exploit, 37(3): 907–921

Li J, Luo X, Shan X Q, Ma C H, Hu G Y, Yan Q T, Liu R E, Chen H H (2005). Natural gas accumulation in the Upper Paleozoic of Ordos Basin, China. Pet Explor Dev, 32(4): 54–58 (in Chinese)

Li S, Tang D Z, Pan Z J, Xu H, Tao S, Liu Y F, Ren P F (2018a). Geological conditions of deep coalbed methane in the eastern margin of the Ordos Basin, China: implications for coalbed methane development. J Nat Gas Sci Eng, 53: 394–402

Li Y, Xu W K, Gao J X, Wu P, Tao C Q, Tian Y, Li J H, Zhang Y L (2021). Mechanism of coal measure gas accumulation under integrated control of "source reservoir-transport system": a case study from east margin of Ordos Basin. J China Coal Soc, 46(8): 2440–2453

Li Y, Xu W K, Wu P, Meng S Z (2020). Dissolution versus cementation and its role in determining tight sandstone quality: a case study from the Upper Paleozoic in northeastern Ordos Basin, China. J Nat Gas Sci Eng, 78: 103324

Li Y, Yang J H, Pan Z J, Meng S Z, Wang K, Niu X L (2019b). Unconventional natural gas accumulations in stacked deposits: a discussion of Upper Paleozoic coal-bearing strata in the east margin of the Ordos Basin, China. Acta Geol Sin (English Edi) 93(1): 111–129

Lu J, Shao L Y, Sun B, Yang M F, Dong D X, Tian W G, Li M P

(2012). Sequence-paleogeography and coal accumulation of Carboniferous-Permian coal measures in the Eastern Ordos Basin. J China Coal Soc, 37(05): 747–754 (in Chinese)

McLimans R K (1987). The application of fluid inclusions to migration of oil and diagenesis in petroleum reservoirs. Appl Geochem, 2(5−6): 585–603

Munz I A (2001). Petroleum inclusions in sedimentary basins: systematics, analytical methods and applications. Lithos, 55(1−4): 195–212

Munz I A, Wangen M, Girard J P, Lacharpagne J C, Johansen H (2004). Pressure-temperature-time-composition (P-T-t-X) constraints of multiple petroleum charges in the Hild field, Norwegian North Sea. Mar Pet Geol, 21(8): 1043–1060

Ouyang Y L, Tian W G, Sun B, Wang B, Qi L, Sun Q P, Yang Q, Dong H C (2018). Characteristics of coal measure gas accumulation and such gas exploration strategies in China. Natural Gas Industry B, 5(5): 444–451

Pedersen K S, Christensen P L (2007). Fluids in hydrocarbon basins. Rev Mineral Geochem, 65(1): 241–258

Qin Y (2018). Research progress of symbiotic accumulation of coal measure gas in China. Natural Gas Industry B, 5(5): 466–474

Qin Y, Shen J, Shi R (2022). Strategic value and choice on construction of large CMG industry in China. J China Coal Soc, 47(1): 371–387 (in Chinese)

Ren Z L, Qi K, Liu R C, Cui J P, Chen Z P, Zhang Y Y, Yang G L, Ma Q (2020). Dynamic background of Early Cretaceous tectonic thermal events and its control on various mineral accumulations such as oil and gas in the Ordos Basin. Acta Petrol Sin, 36(4): 1213–1234 (in Chinese)

Shao L Y, Wang X T, Wang D D, Li M P, Wang S, Li Y J, Shao K, Zhang C, Gao C X, Dong D X, Cheng A G, Lu J, Ji C W, Gao D (2020). Sequence stratigraphy, paleogeography, and coal accumulation regularity of major coal-accumulating periods in China. Int J Coal Sci Technol, 7(2): 240–262

Shao L Y, Zheng M Q, Hou H H, Dong D X, Wang H S (2018). Characteristics sequence-palaeogeography and coal accumulation of Permo-Carboniferous coal measures in Shanxi Province. Coal Sci Techn, 46(02): 1–8+34 (in Chinese)

Shen J, Li K X, Zhang H W, Shabbiri K, Hu Q, Zhang C (2021). The geochemical characteristics, origin, migration and accumulation modes of deep coal-measure gas in the west of Linxing block at the eastern margin of Ordos Basin. J Nat Gas Sci Eng, 91: 103965

Shu Y, Lin Y X, Liu Y, Yu Z Y (2019). Control of magmatism on gas accumulation in Linxing area, Ordos Basin, NW China: evidence from fluid inclusions. J Petrol Sci Eng, 180: 1077–1087

Steele-MacInnis M, Lecumberri-Sanchez P, Bodnar R J (2012). HokieFlincs_H_2O-NaCl: a Microsoft Excel spreadsheet for interpreting microthermometric data from fluid inclusions based on the PVTX properties of H_2O-NaCl. Comput Geosci, 49: 334–337

Su N N, Song F, Qiu L W, Zhang W (2021). Diagenetic evolution and densification mechanism of the Upper Paleozoic tight sandstones in the Ordos Basin, northern China. J Asian Earth Sci, 205: 104613

Sweeney J J, Burnham A K (1990). Evaluation of a simple model of vitrinite reflectance based on chemical kinetics. AAPG Bull, 74: 1559–1570

Tang S L, Tang D Z, Li S, Geng Y G, Xu H, Tao S, Ma L, Zhu X G (2018). Geochemical characteristics and origin of natural gas and gas-filling mode of the Paleozoic in the Yanchuannan gas field, Ordos Basin, China. J Nat Gas Sci Eng, 49: 286–297

Tang S L, Tang D Z, Liu S M, Li S, Tang J C, Wang M F, Zhang A B, Pu Y F (2022). Multiscale pore characterization of coal measure reservoirs and gas storage and transport behavior in Yanchuannan gas field of China. AAPG Bull, 106(12): 2387–2415

Tao S, Chen S D, Pan Z J (2019). Current status, challenges, and policy suggestions for coalbed methane industry development in China: a review. Energy Sci Eng, 7(4): 1059–1074

Volk H, George S C (2019). Using petroleum inclusions to trace petroleum systems-a review. Org Geochem, 129: 99–123

Wei C T, Qin Y, Wang G G X, Fu X H, Zhang Z Q (2010). Numerical simulation of coalbed methane generation, dissipation and retention in SE edge of Ordos Basin, China. Int J Coal Geol, 82(3−4): 147–159

Wygrala B P (1989). Integrated Study of An Oil Field in the Southern Po Basin, Northern Italy. Dissertation for Doctoral Degree. Jülich: Köln University, Research Centre Jülich, 2313: 217

Xu F Y, Wang C W, Xiong X Y, Li S G, Wang Y B, Guo G S, Yan X, Chen G J, Yang Y, Wang H Y, Feng K, Wu P, Liu Y H (2022). Deep (layer) coalbed methane reservoir forming modes and key technical counter measures: taking the eastern margin of Ordos Basin as an example. China Offshore Oil and Gas, 34(4): 30–42+262 (in Chinese)

Xu H, Cao D Y, Li Y, Liu J C, Niu X L, Zhang Y, Qin G H (2016). Geochemical and preliminary reservoir characteristics of the Carboniferous-Permian coal-bearing strata in the Junger Area, Northeastern Ordos Basin, China: source implications for unconventional gas. Energy Fuels, 30(9): 6947–6957

Xu H, Tang D Z, Zhang J F, Yin W, Zhang W Z, Lin W J (2011). Factors affecting the development of the pressure differential in Upper Paleozoic gas reservoirs in the Sulige and Yulin areas of the Ordos Basin, China. Int J Coal Geol, 85(1): 103–111

Yan T T, Yao Y B, Liu D M (2015). Critical tectonic events and their geological controls on gas generation, migration, and accumulation in the Weibei coalbed methane field, southeast Ordos basin. J Nat Gas Sci Eng, 27: 1367–1380

Yan X, Xu F Y, Nie Z H, Kang Y S (2021). Microstructure characteristics of Daji area in east Ordos Basin and its control over the high yield dessert of CBM. J China Coal Soc, 46(8): 2426–2439 (in Chinese)

Yu K, Ju Y W, Qi Y, Huang C, Zhu H J (2020). Geological process of Late Paleozoic shale gas generation in the eastern Ordos Basin, China: revelations from geochemistry and basin modeling. Int J Coal Geol, 229: 103569

Yu Q, Ren Z L, Li R X, Wang B J, Qin X L, Tao N (2017). Paleogeotemperature and maturity evolutionary history of the source rocks in the Ordos Basin. Geol J, 52(S1): 97–118

Zeng X, Wang W, Cao Q, Zhou S W, Dong G D, Wang A M, Chen Z X, Mei H (2022). Evaluation of the accumulation conditions and favorable areas of shale gas in the Upper Palaeozoic marine-continental transitional facies in the Daning-Jixian Area, Ordos Basin. Geofluids, 2414506

Zhang C L, Zhang J Q, Song Z H, Jiang F J, Fan L Y, Pei Y (2021). Gas accumulation conditions and resource potential in coal measure strata of the Permian Shanxi Formation in the eastern Ordos Basin. China Petroleum Exploration, 26: 110–124

Zhang D Y, Zhu J, Zhao X L, Gao X, Geng M, Chen G, Jiao J, Liu S T (2018). Dynamic assessment of coalbed methane resources and availability in China. J China Coal Soc, 43: 1598–1604 (in Chinese)

Zhang Q, Qiu Z, Zhao Q, Zhang L F, Dong D Z, Wang Y M, Hou W, Li S X, Li X T (2022b). Composition effect on the pore structure of transitional shale: a case study of the Permian Shanxi Formation in the Daning-Jixian Block at the eastern margin of the Ordos Basin. Front Earth Sci (Lausanne), 9: 802713

Zhang Y Y, Jiang S, He Z L, Wang Y B, Guo M Q, Zhu G H, Cai D S, Lu S F, Xiao D S, Li Y C, Chen G H (2022c). Characteristics of heterogeneous diagenesis and modification to physical properties of Upper Paleozoic tight gas reservoir in eastern Ordos Basin. J Petrol Sci Eng, 208: 109243

Zhang Y, Li S, Tang D Z, Liu J C, Lin W J, Feng X, Ye J C (2022a). Geological and engineering controls on the differential productivity of CBM wells in the Linfen block, southeastern Ordos Basin, China: insights from geochemical analysis. J Petrol Sci Eng, 211: 110159

Zhao J Z, Zhang W Z, Li J, Cao Q, Fan Y F (2014). Genesis of tight sand gas in the Ordos Basin, China. Org Geochem, 74: 76–84

Zou C N, Yang Z, Huang S P, Ma F, Sun Q P, Li F H, Pan S Q, Tian W G (2019). Resource types, formation, distribution and prospects of coal-measure gas. Pet Explor Dev, 46(3): 451–462